PCCP

Accepted Manuscript

ROYAL SOCIETY OF CHEMISTRY

www.rsc.org/pccp

Physical Chemistry Chemical Physics

ARTICLE

Spin-orbit coupling effects on electronic structures in stanene nanoribbons

Wenqi Xiong,[a] Congxin Xia,*[a] Yuting Peng,[b] Juan Du,[a] Tianxing Wang,[a] Jicai Zhang[a] and Yu Jia[c]

Received 00th January 20xx,
Accepted 00th January 20xx

DOI: 10.1039/x0xx00000x

The electronic structures and magnetic properties of stanene nanoribbons (SnNRs) are studied by using first-principles calculations, considering the spin-orbit coupling (SOC) effects and edge passivation. The results show that all considered armchair SnNRs are nonmagnetic semiconductors with the gap values as a periodic oscillation function of ribbon width. The zigzag SnNRs present the antiferromagnetic ground states with opposite spin order between the two edges, and the gaps decrease as the ribbon widths increase. Moreover, the influences of dangling bonds are obvious on the ferromagnetic magnetic moments of zigzag SnNRs. In addition, the SOC effects can open the band gap values of stanene sheets and zigzag SnNRs, while reduce the band gap of armchair SnNRs, which indicate that stanene nanostructures may be applied in the spinelectronics and quantum spin Hall fields.

1 Introduction

As the rise of graphene,[1-5] different kinds of two-dimensional (2D) atomic layer materials manifest many new and interesting properties not found in bulk materials, such as 2D MoS_2[6-10] and phosphorene.[11-14] Among these new studied 2D nanomaterials, one particular topic of interest is exploring the electronic characteristics of group IV elements-based 2D materials except graphene. So far, extensive studies have shown that 2D silicene and germanene analogues of silicon and germanium possess the promising applications in electronic applications.[15-18] More recently, a new 2D material Sn monolayer called stanene has also been firstly fabricated by growing on suitable Bi_2Te_3(111) substrate,[19] which will attract much attention due to its novel electronic characteristics.

For the studies of stanene, Song et al. firstly predicted theoretically the existence of stanene because Sn also belongs to group IV in the periodic table and the Fermi velocity of freestanding stanene is about 0.55×10^6 ms^{-1} considering spin-orbital coupling (SOC) effects.[20] The studies of Cai et al. showed that stable stanene has a similar hexagonal buckled monolayer structure to graphene and silicene with a remarkable 72 meV bandgap.[21] The influences of strain on the band structures are investigated by means of first-principles methods.[22] Based on first-principles calculations, Xu et al. applications at room temperature.[23] Moreover, some studies reported that the stable epitaxial growth of stanene can be realized on substrate and render stanene feasible use as a topological insulator.[24,25] Broek et al. studied Sn nanoribbons have earlier current onsets and carry currents 20% larger than C/Si/Ge-nanoribbons.[26] In addition, although experimental studies on stanene about growth mechanism are scarce, previous properties and substrate effects studies on graphene and silicene can pave the way to production and application of stanene.[27-32] These studies indicate that the new 2D stanene-based nanomaterials have a promising applications on nano-electronic devices.

It is well known that finite size nanoribbons materials play an extremely critical role on the related theoretical and experimental studies. However, to our knowledge, there are few works on the electronic structures and magnetic properties of stanene nanoribbons (SnNRs) to date. Compared to graphene (silicene and germanene)-based nanoribbons systems,[33-35] how about the effects of ribbon widths and edge states on the electronic and magnetic properties of SnNRs? To reveal this question, in this paper, we systematically studied the electronic structures and magnetic properties of bare and hydrogenated armchair stanene nanoribbons (ASnNRs) and zigzag stanene nanoribbons (ZSnNRs) by means of the first-principles calculations, considering the SOC effects.[20,24,25]

[a]Department of Physics, Henan Normal University, Xinxiang, Henan 453007, China
[b]Department of Physics, University of Texas at Arlington, Texas 76019, USA
[c]School of Physics and Engineering, Zhengzhou University, Zhengzhou 450052, China.
E-mail:xiacongxin@htu.edu.cn

2 Computational method

In this work, spin-polarized density functional calculations are carried out with the Vienna *ab initio* simulation package (VASP).[36,37] The exchange–correlation functional is treated by the generalized gradient approximation (GGA) with Perdew-Burke-Ernzerhofer parameterization (PBE).[38] The projected augmented wave potential is also employed to describe the electron-ion potential.[39] The kinetic energy cutoff of plane wave is set to be 300 eV for the plane wave expansion. The 15×15×1, 1×20×1 and 20×1×1 k-point meshes are used for the Brillouin zone (BZ) integration in the stanene nanosheets, ASnNRs and ZSnNRs,[40] respectively. In addition, the 2D crystal as well as the 1D nanoribbons are simulated with a supercell approach. Moreover, in order to avoid artificial interactions between the periodic images of the structures, the vacuum space of at least 20 Å is added. The SOC is calculated by a second-variation procedure.[41] All atomic positions are fully relaxed using the conjugated gradient method until the Hellmann-Feynman force on each atom is less than 0.01eV/Å. Moreover, the convergence for energy is chosen as 10^{-5} eV between two steps.

3 Results and discussion

3.1 Electronic structures of bare SnNRs

As a benchmark test for our approach and parameterization, our systematic studies begin with calculating the structural parameters and electronic properties of stanene. As shown in Fig. 1, the optimized stanene structure is a 2D hexagonal crystal with a lattice constant a=4.674Å. In contrast to graphene, silicene and germanene, the 2D stanene has a larger buckling amplitude of Δ = 0.85 Å. These calculations are in agreement with previous calculations.[20,42,43] In addition, the calculated band structures along high symmetry directions of the first BZ are also plotted in Fig. 1(c). It can be seen that the linear Dirac-like dispersion appears around the high-symmetric K point of the BZ, which is similar as that of graphene, silicene and germanene.[4,44] Moreover, the valence band maximum (VBM) and conduction band minimum (CBM) locate at K points, which indicates that the 2D stanene is a direct gap semiconductor. In particular, we also find that the 2D stanene possesses nearly zero band gap in the absence of SOC effects; however, a large direct band gap value (73 meV) can be obtained (see insert Figs of Fig. 1) in the presence of SOC effects, which is in good agreement with previous results.[20,21] These results show that in the stanene, the SOC effects on electronic strcutrures are much more obvious than that in the graphene and silicene.[20] Therefore, the above calculated results of 2D stanene indicate that the selected calculation methods are reliable for the following studies of stanene nanoribbons systems.

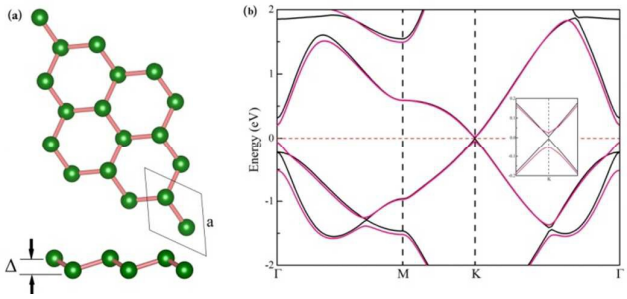

Fig. 1 (a) The top and side views of the buckled stanene sheet, the hexagonal lattice constant a and buckling amplitude Δ. (b) The band structure of stanene without (black solid lines) and with (pink solid lines) the SOC effects. The inset of (b) shows a zoomed in energy dispersion near the K point. The Fermi level is set to zero energy and marked by the red dashed line.

3.2 Electronic structures and magnetism of ASnNRs

In the following sections, we study the structural and electronic properties of stanene nanoribbons, which is modeled by cutting a 2D stanene sheets along armchair and zigzag orientations, as shown in Fig. 2. The ribbons are denoted as N_a-ASnNRs and N_z-ZSnNRs with N_a and N_z characterizing the ribbon widths. Moreover, the effects of edge and hydrogen passivation on the band structures and magnetic properties also considered.

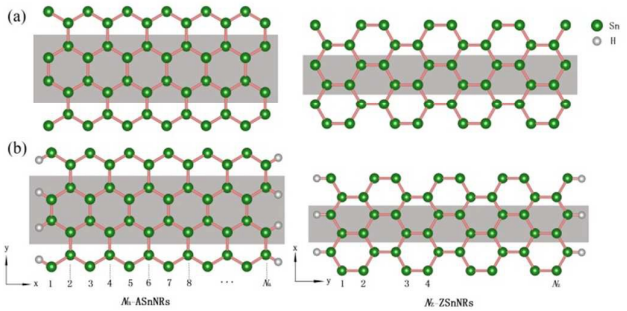

Fig. 2 The geometric structures of (a) bare N_a-ASnNRs and N_z-ZSnNRs, (b) hydrogenated N_a-ASnNRs and N_z-ZSnNRs. The shaded area represents the unit cell. The green and gray balls represent Sn and H atoms, respectively.

Fig. 3 displays the variation of total energy as a function of ribbon width for bare and hydrogenated ASnNRs. Numerical results show that whether the edge is hydrogenated or not, the total energies of the ASnNRs decrease linearly with increasing ribbon widths. Moreover, it can be seen that the total energies of hydrogenated ASnNRs are always lower than that of bare ASnNRs for same widths, which indicate that the hydrogenated ASnNRs are more stable than that of bare ASnNRs. Therefore, in the following, we will study the electronic structures of hydrogenated ASnNRs in more detail.

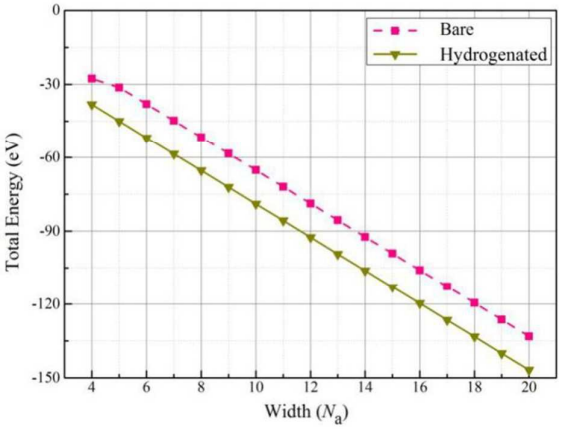

Fig. 3 The total energies are calculated as functions of the ribbon widths N_a in the bare and hydrogenated ASnNRs.

In addition, in order to study the stability of SnNRs, according to previous studies,[29,45-47] we also calculate the edge energy:

$$E_{edge} = \left(E_{ribbons} - mE_{unit}\left(stanene\right) - n\mu_H\right)/2L \quad (1)$$

where $E_{ribbons}$ is the total energy of the SnNRs, and E_{unit} is the energy of the monolayer stanene. μ_H is energy of a hydrogen atom in the H_2 molecule. The *m* and *n* are the numbers of stanene units and hydrogen atoms in the nanoribbons, respectively. *L* is the length of nanoribbons. Note that in formula (1) we divided by 2*L*, because the unit cell contains both edges of the SnNRs. From the calculated the edge energies of the bare and hydrogenated ASnNRs (Fig. 4(a)), the edge energies converge to a constant. The edge energies of the hydrogenated ASnNRs are slightly lower than that of bare edge SnNRs. Therefore, the hydrogenated ASnNRs are more stable than the ASnNRs with bare edges, because of their relatively higher edge energies.

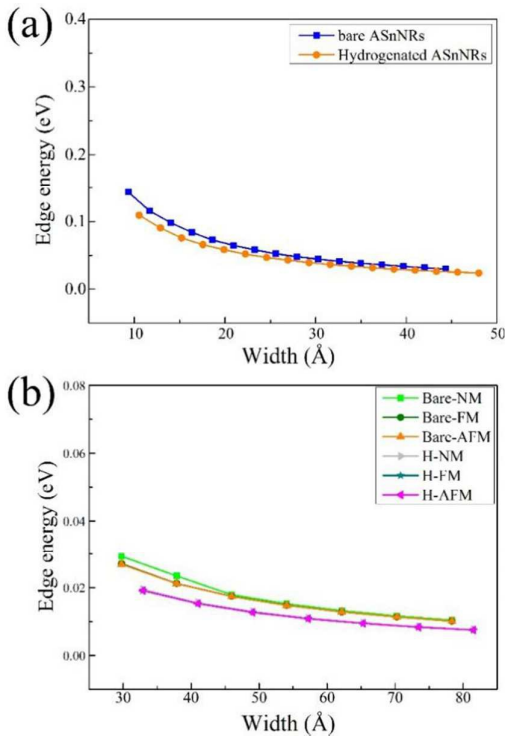

Fig. 4 (a) The calculated edge energies of the ASnNRs with bare and hydrogenated edges. (b) The edge energies of bare and hydrogenated ZSnNRs for NM, FM and AFM states, respectively.

In order to understand the electronic characteristics of ASnNRs, we calculate the electronic band structures of bare and hydrogenated ASnNRs, considering the SOC effects and different ribbon widths N_a from 4 to 20. Fig. 5 shows that for all considered ASnNRs, the spin-up and spin-down band structures are symmetric and possess the nonmagnetic ground states. Moreover, for hydrogenated ASnNRs, the VBM and CBM locate at Γ point, which indicate hydrogenated ASnNRs are the direct gap semiconductors. These behaviors are similar as previous results of graphene and silicene nanoribbons.[33,34] Here we also note that for bare ASnNRs cases, the indirect band gaps occur when the widths are smaller than 2.1 nm (the widths along x-axis) such as 7-ASnNRs shown in Fig.6(a). The reason can be explained as follows. The smaller ribbon width is, the stronger interedge coupling are. The dangling bonds of edge atoms for unstable bare ASnNRs may cause the edge reconstruction and different charge density. Thus, the behavior may be induced by dangling bonds of ribbon edge and the interedge coupling in the ASnNRs. In addition, Fig. 5(c) also shows that when we take the SOC effects into our calculations of hydrogenated ASnNRs, the band dispersion take place some changes. The direct gaps located at Γ point decrease a little because of band split. Therefore, the SOC effects exercises great influence on the electronic band structure of 2D stanene nanosheet, while the influence is small on the band gap of 1D SnNRs. Although the SOC effects do not result in a remarkable change in band dispersion, our calculations provide more detail to study the QSH effects for stanene-based nanomaterials.

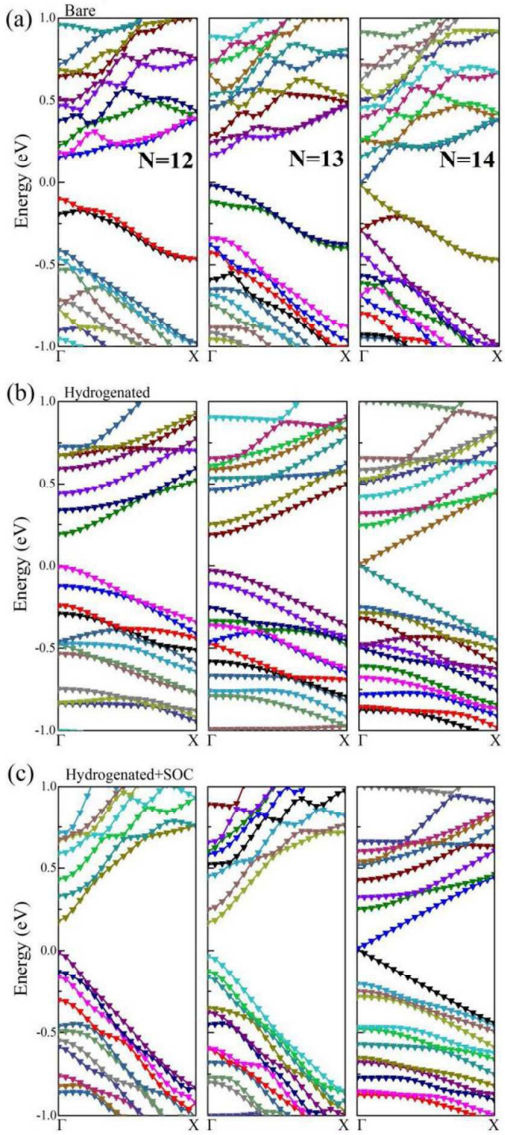

Fig. 5 The band structures of (a) bare N_a-ASnNRs without SOC effects, (b) hydrogenated N_a-ASnNRs without SOC effects, and (c) hydrogenated N_a-ASnNRs with SOC effects for N_a=12, 13, and 14, respectively. The Fermi level is set at zero.

In Fig. 6(b), the band gaps of the ASnNRs are investigated as a function of ribbon widths. It can be clearly seen that the band gaps present an oscillation behavior with the variation of the ribbon width. According to the gap variation, the N_a-ASnNRs can be classified into three families with N_a = 3n, 3n + 1, 3n +2, where n is a positive integer. We can see from Fig. 6(b) that for hydrogenated ASnNRs with and without SOC effects, the band gap values behave a regular pattern as $\Delta_{3n+1} > \Delta_{3n} > \Delta_{3n+2}$(n>1). Furthermore, the band gap values for the ribbon widths N_a = 3n + 2 are smaller than 40 meV, but the hydrogenated ASnNRs don't become metal with increasing the ribbon widths. Moreover, Fig. 6 also shows that the slight decrease of band gap is induced by the SOC effects due to band splitting in the hydrogenated ASnNRs, as expected. In particular, we can also see from Fig. 5 that for bare ASnNRs case, the gaps behave a hierarchy as $\Delta_{3n} > \Delta_{3n+1} > \Delta_{3n+2}$ (n>1), which is different from that of hydrogenated ASnNRs. Note that for bare and hydrogenated ASnNRs, the differences of the band gap versus the ribbon widths are similar as the electronic behaviors of bare and hydrogenated BN armchair nanoribbons.[48] Therefore, these results indicate that the ribbon edge and width are important factors in the studies of ASnNRs.

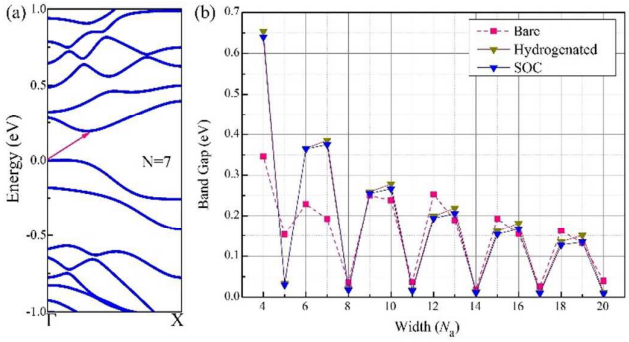

Fig. 6 (a) The band structure of bare 7-ASnNRs. (b) The variation of band gaps as a function of ribbon widths N_a for bare N_a-ASnNRs without SOC effects, hydrogenated N_a-ASnNRs without SOC effects and hydrogenated N_a-ASnNRs with SOC effects, respectively.

3.3 Electronic structures and magnetism of ZSnNRs

In order to understand the electronic characteristics of ZSnNRs and solve the question whether the magnetic moments can be raised in the ZSnNRs, we carry out the calculations of total energies and band structures of the ZSnNR considering nonmagnetic (NM), ferromagnetic (FM) and antiferromagnetic (AFM) orders. Numerical results show that the total energies of AFM and FM states are lower than that of NM states for any width of the ZSnNR, indicating that spin polarization is a possible stabilization mechanism for the ZSnNRs.

In addition, to explore the stability of AFM and FM states in the ZSnNRs, in Fig. 7(a), we also present the total energy differences $\Delta E = E_{FM} - E_{AFM}$ as a function of the ribbon width. This is a key component in understanding the spin polarization of the nanoribbons, which is directly related to the interedge interaction and determines the spin alignment at the edges. It can be seen from Fig. 7(a) that for all considered cases, the total energy differences are positive value, which indicates that the total energy of AFM states is lower than that of FM states and the NM states in the bare and hydrogenated ZSnNRs. Therefore the ZSnNRs possess AFM ground state for different ribbon widths. Meanwhile, Fig. 7(a) also shows that the total energy differences between the FM and AFM spin configurations decrease when the ribbon widths increase and eventually vanish. Moreover, for bare ZSnNRs, the total energy difference decreases rapidly with increasing ribbon widths; while for hydrogenated N_z-ZSnNRs, the total energy difference decreases slowly with increasing the ribbon width N_z. For instance, the total energy difference ΔE of bare N_z-ZSnNRs reduces 9.8 meV for N_z from 8 to 20, but changes 2 meV for hydrogenated N_z-ZSnNRs. This result agrees with the calculated edge energies of bare and hydrogenated ZSnNRs in NM, FM, and AFM states (Fig. 4(b)). Moreover, three states for hydrogenated ZSnNRs possess lower edge energies than that of bare ones, which indicates the hydrogenated ZSnNRs are more stable.

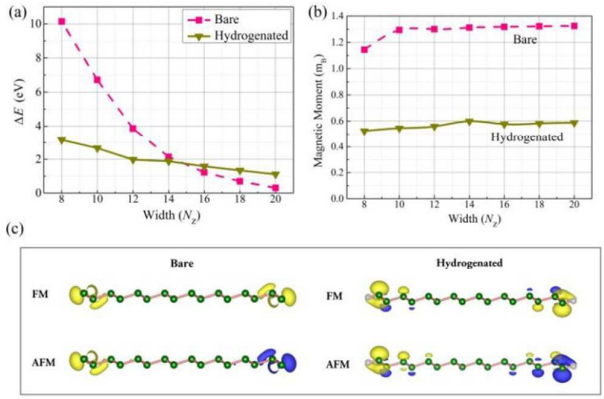

Fig. 7 (a) The total energy differences $\Delta E = E_{FM} - E_{AFM}$ and (b) magnetic moments of the FM states as a function of width N_z in the bare and hydrogenated N_z-ZSnNRs, respectively. (c)The spin densities of bare and hydrogenated 8-ZSnNRs in FM states and AFM states, respectively. Yellow (blue) distributions represent positive (negative) values. The isosurface level is taken as 0.007 e/Å^3.

In order to understand the mechanism of spin polarization and the origin of the magnetism in the ZSnNRs, we further calculate the magnetic moments and spin density of bare and hydrogenated ZSnNRs for different widths N_z. In Fig. 7(b), it is interesting to find that the magnetic moments are insensitive to the change of ribbon widths in bare and hydrogenated ZSnNRs. In addition, the magnetic moments of bare N_z-ZSnNRs are still larger than that of hydrogenated ZSnNRs for all considered widths N_z. Fig. 7(c) also provide the side view of spin density of 8-ZSnNRs as an example. It can be seen clearly that the magnetic moments are mainly contributed by edge atoms and decrease quickly towards the center of the ribbon. For FM states, the majority spins are only found at two edges of the bare 8-ZSnNRs; while most majority spins and few minority spins exist at hydrogenated 8-ZSnNRs, which weaken the magnetic moments. So the magnetic moments of bare N_z-ZSnNRs are still larger than hydrogenated one. The fundamental reason is that the dangling bonds at ZSnNRs are removed by H atoms. The presence of a dangling bonds is crucial form the magnetism of ZSnNRs. However, for AFM states, the equal majority spins and minority spins occupy the each edge atoms of ZSnNRs.

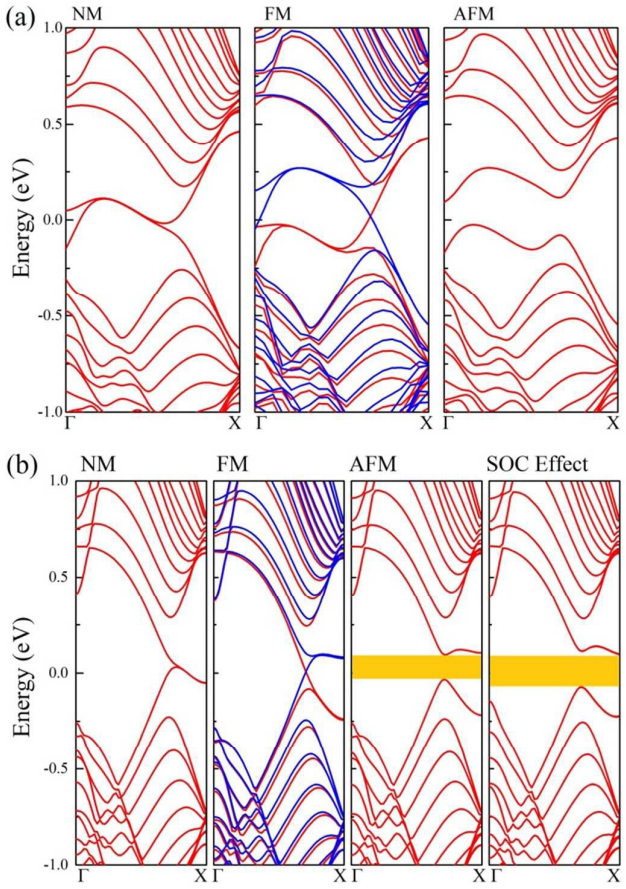

Fig. 8 (a) The band structures of bare 12-ZSnNRs without SOC effects in NM states, FM states, and AFM states, respectively. (b) The band structures of hydrogenated 12-ZSnNRs in NM states, FM states, AFM states without SOC effects, and AFM states with SOC effects, respectively. The Fermi level is set at zero.

To further understand the influences of edge states and SOC effects on the electronic structures of ZSnNRs, the band structures of NM, FM and AFM states are calculated. As an example, in Fig. 8(a) and (b), we present the energy band structures at NM, FM and AFM states of the bare and hydrogenated 12-ZSnNRs. Numerical results show that for NM states of bare and hydrogenated ZSnNRs, two energy bands across the Fermi level, which results in metallic character in NM states. Also, the spin polarized FM states of the ZSnNRs presents asymmetrical majority spin and minority spin bands, which means the spin degeneracy has been broken. Both spin channels for FM states show a metallic characteristics regardless of the ribbon widths. For the AFM states, the conduction band edge and valence band edge are split just above and below the Fermi level, resulting in a small band gap with the value of 0.11 eV for bare 12-ZSnNRs and 0.13 eV for hydrogenated 12-ZSnNRs without SOC effects. Moreover, in the AFM configuration, the opposite spin states at opposite edges occupy different sublattices induces staggered sublattice potentials, which results in the change of band gaps for electrons on hexagonal lattices. In addition, the SOC effects are implemented into the hydrogenated ZSnNRs calculations of band gaps in AFM states to study the influence on the band structures. Fig. 8(b) shows that the CBM and VBM are shifted up and down, which results in the increase of band gap from 0.13 eV to 0.17 eV for 12-ZSnNRs in the presence of SOC effects. In addition, we also considering the SOC effects in ZSnNRs for FM states in Fig.9. The results show that for bare ZSnNRs, it remains the metallic character in the presence of SOC effects. However, for hydrogenated ZSnNRs, the SOC effects induce the remarkable band gap of 55 meV. Therefore, the SOC effects have obvious influences on electronic properties for hydrogenated ZSnNRs.

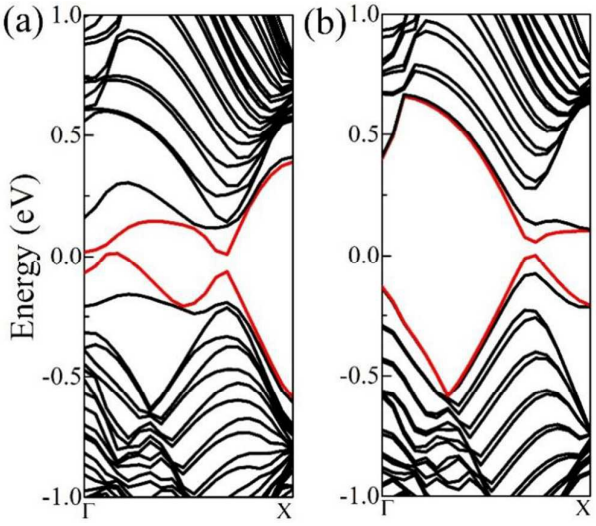

Fig. 9 The band structures of (a) bare and (b) hydrogenated 12-ZSnNRs with SOC effects in FM states, respectively. The Fermi level is set at zero.

Moreover, we notice a remarkable changes from Fig. 8 by comparing the band gap types of bare ZSnNRs with the case of hydrogenated ZSnNRs. We see clearly that the AFM case of hydrogenated ZSnNRs has a direct gap for different widths N_z we have considered which highly correspond to graphene nanoribbbons and silicene nanoribbons.[49,50] While bare ZSnNRs also possess indirect gap in AFM states. The reason is that unstable edge atoms induce the change of electronic structure in the absence of SOC effects.

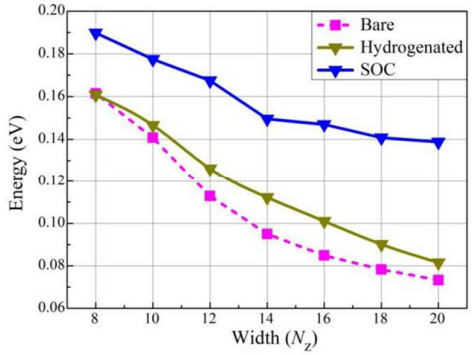

Fig. 10 Variation of the band gaps in AFM states for bare N_z-ZSnNRs without SOC effects, hydrogenated N_z-ZSnNRs without SOC effects, and hydrogenated N_z-ZSnNRs with SOC effects, respectively.

In Fig. 9, we present the band gaps dependence on the ribbon widths for the bare and hydrogenated N_z-ZSnNRs with the AFM states, considering the presence and absence of SOC effects. Numerical results show that the band gap values decrease with increasing the ribbon widths, as expected. The reason is that

quantum confinement effects are weakened when quantum size increases in the bare and hydrogenated ZSnNRs. Moreover, Fig. 9 also shows that the band gap values decreases when the ribbon width increases in the bare and hydrogenated ZSnNRs. For bare N_z-ZSnNRs case, the band gaps reduce from 0.16 eV for 8-ZSnNRs to 0.07 eV for 20-ZSnNRs. Also, in the case of hydrogenated N_z-ZSnNRs, the band gaps decrease from 0.16 eV for 8-ZSnNRs to 0.08 eV for 20-ZSnNRs. In particular, we can also find from Fig. 8 that for each considered ZSnNRs case, the SOC effects enhance the band gap values in the bare and hydrogenated ZSnNRs. These results indicate that SOC effects are very important to SnNRs and related device applications.

4. Conclusions

In summary, we have investigated the electronic structures and magnetic properties of SnNRs with armchair and zigzag edges by means of first-principles methods. Moreover, the SOC effects and edge passivation are also considered. Numerical results show that ASnNRs are NM semiconductors with bare and hydrogenated edges, and the gap values present a periodic oscillation function of ribbon width. In addition, results also show that the bare and hydrogenated ZSnNRs present the AFM ground-state semiconducting properties with opposite spin order between the two edges, and the gap values decrease as the ribbon widths increase. Moreover, the influences of dangling bonds are obvious on the FM magnetic moments of ZSnNRs. In particular, it can be seen that the SOC effects can open the band gap values of stanene sheets and zigzag SnNRs, while reduces the band gap of ASnNRs. We expect that these results are useful to understand the new graphene-like stanene as promising applications in nanoelectronics and quantum spin Hall fields.

We would also like to point out that although conventional DFT methods underestimate the band gap of semiconductors, DFT methods are good at predicting correct trends and physical mechanisms. Thus, for future related experimental studies, the numbers obtained in this work should be taken with care since the calculated energy gap is underestimated.

Acknowledgements

This research was supported by the National Natural Science Foundation of China under Grant No.U1304518 and 91233120. The calculations are also supported by The High Performance Computing Center of Henan Normal University.

References

1 K. S. Novoselov, A. K. Geim, S. V. Morozov, D. Jiang, M. I. Katsnelson, I. V. Grigorieva, S. V. Dubonos and A. A. Firsov, *Nature*, 2005, **438**, 197-200.

2 X. S. Li, W. W. Cai, J. An, S. Kim, J. Nah, D. X. Yang, R. Piner, A. Velamakanni, I. Jung, E. Tutuc, S. K. Banerjee, L. Colombo and R. S. Ruoff, *Science*, 2009, **324**, 1312-1314.

3 S. Das Saema, S. Adam, E. H. Hwang and E. Rossi, *Rev. Mod. Phys.*, 2011, **83**, 407.

4 A. H. Castro Neto, F. Guinea, N. M. R. Peters, K. S. Novoselov and A. K. Geim, *Rev. Mod. Phys.*, 2009, **81**, 109.

5 J. H. Yang, R. X. Li, N. J. Huo, W. L. Ma, F. Y. Lu, C. Fan, S. X. Yang, Z. M. Wei, J. B. Li, and S. S. Li, *RSC Adv.* 2014, **4**, 49873.

6 N. J. Huo, Z. M. Wei, X. Q. Meng, J. Kang, F. M. Wu, S. S. Li, S. H. Wei and J. B. Li, *J. Mater. Chem. C*, 2015, **3**, 5467-5473.

7 C. Fan, T. Li, Z. M. Wei, N. J. Huo, F. Y. Lu, J. H. Yang, R. X. Li, S. X. Yang, B. Li, W. P. Hu and J. B. Li, *Nanoscale*, 2014, **6**, 14652-14656.

8 K. F. Mak, C. Lee, J. Hone, J. Shan and T. F. Heinz, *Phys. Rev. Lett*., 2010, **105**, 136805.

9 T. Korn, S. Heydrich, M. Hirmer, J. Schmutzler, and C. Schuller, *Appl. Phys. Lett.*, 2011, **99**, 102109.

10 Q. Yue, J. Kang, Z. Z. Shao, X. A. Zhang, S. L. Chang, G. Wang, S. Q. Qin, and J. B. Li, *Phys. Lett. A* 2012, **376**, 1166.

11 H. Liu, A. T. Neal, Z. Zhu, Z. Luo, X. F. Xu, D. Tomanek and P. D. Ye, *ACS Nano*, 2014, **8**, 4033-4041.

12 A. S. Rodin, A. Carvalho and A. H. Castro Neto, *Phys. Rev. Lett.*, 2014, **112**, 176801.

13 Y. Li, S. X. Yang and J. B. Li, *J. Phys. Chem. C*, 2014, **118**, 23970-23976.

14 Y. Li, Z. M. Wei and J. B. Li, Appl. Phys. Lett., 2015, **107,** 112103.

15 S. Lebègue and O. Eriksson, *Phys. Rev. B*, 2009, **79**, 1154009.

16 L. Chen, C. C. Liu, B. J. Feng, X. Y. He, P. Cheng, Z. J. Ding, S. Meng, Y. G. Yao and K. H. Wu, *Phys. Rev. Lett.*, 2012, **109**, 056804.

17 Z. Y. Ni, Q. H. Liu, K. C. Tang, J. X. Zheng, J. Zhou, R. Qin, Z. X. Gao, D. P. Yu and J. Lu, *Nano Lett.*, 2012, **12**, 113-118.

18 C. J. Tabert, E. J. Nicol, *Phys. Rev. Lett.*,2013, **110**, 197402.

19 F. F. Zhu, W. J. Chen, Y. Xu, C. L. Gao, D. D. Guan, C. H. Liu, D. Qian, S. C. Zhang and J. F. Jia, *Nat. Mater.* 2015, **14**, 1020-1025.

20 L. Matthes, O. Pulci and F. Bechstedt, *J. Phys.: Condens. Matter*, 2013, **25**, 395305.

21 B. Cai, S. Q. Zhang, Z. Y. Hu, Y. H. Hu, Y. S. Zou and H. B. Zeng, P*hys. Chem. Chem. Phys.*, 2015, **17**, 12634-12638.

22 M. Modarresi, A. Kakoee, Y.Mogulkoc and M. R. Roknabadi, *Comp. Mater. Sci.*, 2015, **101**, 164-167.

23 Y. Xu, B, H. Yan, H. J. Zhang, J. Wang, G. Xu, P. Z. Tang, W. H. Duan, and S. C. Zhang, *Phys. Rev. Lett.*, 2013, **111**, 136804.

24 Y. M. Fang, Z. Q. Huang, C. H. Hsu, X. D. Li, Y. X. Xu, Y. H. Zhou, S. Q. Wu, F. C. Chuang and Z. Z. Zhou, *Sci. Rep.*, 2015, **5**, 14196.

25 Y. Xu, P. Z. Tang and S. C. Zhang, *Phys. Rev. B*, 2015, **92**, 081112.

26 B. Van Den Broek, M. Houssa, G. Pourtois, V. V. Afanasev, and A. Stesmans, *Phys. Status. Solidi (R),* 2014, **8**, 931-934.

27 J. F. Gao, J. F. Zhang, H. S. Liu, Q. F. Zhang, and J. J. Zhao, *Nanoscale*, 2013, **5**, 9785-9792.

28 H. S. Liu, J. F. Gao, and J. J. Gao, *J. Phys. Chem. C*, 2013, **117**, 10353-10359.

29 L. Tao, E. Cinquanta, D. Chiappe, C. Grazianetti, M. Fanciulli, M. Dubey, A. Molle, and D. Akinwande, *Nat. Nanotechnol.* 2015, **10**, 227-231.

30 J. F. Gao, and F. Ding, *J. Phys. Chem. C*, 2015, **119**, 11086-11093.

31 J. F. Gao, and J. J. Zhao, *Sci. Rep.* 2012, **2**, 861.

32 A. Khan, L. Yang, J. Xu, L. Y. Jin, and Y. J. Zhang, *Angew. Chem. Int. Ed.*, 2014, **53**, 11257-11260.

33 V. Barone, O. Hod and G. E. Scuseria, *Nano Lett.*, 2006, **6**, 2748-2754.

34 Y. L. Song, Y. Zhang, J. M. Zhang and D. B. Lu, *Appl. Surf. Sci*., 2010, **256**, 6313-631.

35 Q. Pang, Y. Zhang, J. M. Zhang, V. Ji and K. W. Xu, *Nanoscale*, 2011, **3**, 4330-4338.

36 G. Kresse and J. Hafner, *Phys. Rev. B* 1994, **49**, 14251.

37 G. Kresse and J. Furthmüller, *Phys. Rev. B* 1996, **54**, 11169.

38 J. P. Perdew, K. Burke and M. Ernzerhof, *Phys. Rev. Lett.* 1996, **77**, 3865.

39 P. E. Blöchl, *Phys. Rev. B*, 1994, **50**, 17953.
40 H. J. Monkhorst and J. D. Pack, *Phys. Rev. B* 1976, **13**, 5188.
41 C. Li, A. J. Freeman, H. J. F. Jansen and C. L. Fu, *Phys. Rev. B* 1990, **42**, 5433.
42 B. Van den Broek, M. Houssa, E. Scalise, G. Pourtois, V. V. Afanas'ev and A. Stesmans, *2D Materials*, 2014, **1**, 021004.
43 A. S. Negreira, W. G. Vandenberghe and M. V. Fischetti, *Phys. Rev. B*, 2015, **91**, 245103.
44 C. C. Liu, W. X. Feng and Y. G. Yao, *Phys. Rev. Lett.*, 2011, **107**, 076802.
45 J. F. Gao, J. J. Zhao, and F. Ding, *J. Am. Chem. Soc.*, 2012, **134**, 6204-6209.
46 P. Koskinen, S. Malola, and H. Häkkinen, *Phys. Rev. Lett.*, 2008, **101**, 115502.
47 J. Kunstmann, C. Özdoğan, A. Quandt, and H. Fehske, *Phys. Rev. Lett.*, 2011, **83**, 045414.
48 M. Topsakal, E. Aktürk and S. Ciraci, *Phys. Rev. B*, 2009, **79,** 115442.
49 Y. W. Son, M. L. Cohen and S. G. Louie, *Phys. Rev. Lett.*, 2006, **97**, 216803.
50 C. Y. Xu, G. F. Luo, Q. H. Liu, J. X. Zheng, Z. M. Zhang, S. Nagase, Z. X. Gao and J. Lu, *Nanoscale***,** 2012, **4**, 3111-3117.